ELSEVIER

Mapping Vegetation, Soils, and Geology in Semiarid Shrublands Using Spectral Matching and Mixture Modeling of SWIR AVIRIS Imagery

Nick A. Drake, Steve Mackin,† and Jeff J. Settle‡*

Spectral matching and linear mixture modeling techniques have been applied to synthetic imagery and AVIRIS SWIR imagery of a semiarid rangeland in order to determine their effectiveness as mapping tools, the synergism between the two methods, and their advantages, and limitations for rangeland resource exploitation and management. Spectral matching of pure library spectra was found to be an effective method of locating and identifying endmembers for mixture modeling although some problems were found with the false identification of gypsum. Mixture modeling could accurately estimate proportions for a large number of materials in synthetic imagery; however, it produced high variance estimates and high error estimates when presented with all nine AVIRIS endmembers because of high noise levels in the imagery. The problem of which endmembers to select was addressed by implementing a mixture model that allowed estimation of the errors on the proportions estimates, discarding the endmembers with the highest errors, recomputing the errors, and the proportions estimates, and iterating this process until the mixture maps were relatively free from noise. This methodology ensured that the lowest contrast materials were discarded. The inevitable confusion that followed was monitored the using the maps produced by spectral matching. Spectral matching was more effective than mixture modeling for geological mapping because it allowed identification and mapping of the relatively pure regions of all the surficial materials that exert an influence on the spectral response. The maps of the different clay minerals were of considerable value for mineral exploration purposes. Conversely, spectral matching was less useful than mixture modeling for rangeland vegetation studies because a classification of all pixels is needed and abundance estimates are required for many applications. Mixture modeling allowed identification of both nonphotosynthetic and green vegetation cover and thus total cover. Though the green vegetation mixture map appears to be very precise, the nonphotosynthetic vegetation estimates were poor. ©*Elsevier Science Inc., 1999*

INTRODUCTION

This study investigates the capabilities, and limitations of using imaging spectroscopy data in the short wavelength infrared (SWIR 2–2.5 μm) to map the vegetation, geology, and soils of a semiarid rangeland. This wavelength range has been shown to be a promising one for mineral identification and mapping (Mackin et al., 1990; Hook et al., 1991), but also has the potential to identify, and map some of the different constituents of the vegetation canopy (i.e., green leaves and woody material) because green plant materials exhibit a spectrum dominated by water absorption while spectra of nonphotosynthetic plant materials exhibit absorption features due to lignin, and hollocellulose (Elvidge, 1990).

To accomplish this aim, we compared and combined two methods of mapping surface materials using imaging spectrometry data. First, we adopted a spectral matching approach to match library spectra to those in the image, in

* Department of Geography, King's College, London
† Departmento Quimica Agricola, Geologia y Geoquimica, Universidad Autonoma, Madrid, Spain
‡ ESSC, University of Reading, Whiteknights, Reading, Berks, United Kingdom.

Address correspondence to N. A. Drake, Dept. of Geography, King's College, Strand, London, WC2R 2LS, UK. E-mail: nick.drake@kcl.ac.uk

Received 4 August 1997; revised 16 September 1998.

REMOTE SENS. ENVIRON. 68:12–25 (1999)

655 Avenue of the Americas, New York, NY 10010

0034-4257/99/$–see front matter
PII S0034-4257(98)00097-2

order to identify materials and derive a classification map of their spatial distribution. Spectral matching was also used to determine the purest pixels of each identified material. This is precisely the prior information needed when applying a linear mixture model, the second approach we investigated. Thus a combined mixture modeling/spectral matching approach is a promising method for estimating the fractional cover of Earth surface materials (Mackin et al., 1990; Kruse et al., 1993a; Ben-Dor and Kruse, 1995).

BACKGROUND AND OBJECTIVES

The information provided by spectral matching and linear mixture modeling of rangelands have applications in studies of geology, soils, and rangeland vegetation exploitation, degradation, and management as outlined below.

Vegetation

Vegetation cover is important for land degradation studies because it exerts a control on evapotranspiration, infiltration, runoff, soil erosion, and, over the long term, the organic matter content of soils. It is also important for grazing management because the amount of green vegetation determines cattle turnout dates and can be used to adjust grazing pressure and determine the amount of forage available for winter grazing (Frank and Aase, 1994).

The most commonly used remote sensing techniques for estimating green vegetation cover are vegetation indices that employ red and infrared wavelengths, such as the normalized difference vegetation index (NDVI). Though some studies of semiarid shrublands have successfully used these vegetation indices (Kennedy, 1989), many studies have shown that they are of limited value (Pickup et al., 1994; Graetz et al., 1986) because of the darkening evident in semiarid vegetation canopies (Ringrose et al., 1994), soil albedo effects (Elvidge and Chen, 1995; Huete et al., 1985), and the fact that some soils exhibit a marked difference in reflectance between the red and NIR due to soil or rock mineralogy (Elvidge and Lyon, 1985). In order to provide a better estimate of vegetation cover in rangelands, a number of new indices have been developed that do not rely on red and infrared reflectance (Ringrose et al., 1994; Graetz et al., 1986; Pickup et al., 1994). However, the relationship between vegetation cover and these indices appears to vary between different areas along an arid humid transition in Northern Australia, and no single index seems to be universally applicable to all semiarid vegetation (Ringrose et al., 1994).

Numerous studies have shown that mixture modeling can be used to estimate vegetation cover (Mackin et al., 1990; Smith et al., 1990; Drake, 1991; Roberts et al., 1993), and Garcia-Haro et al. (1996) have shown that mixture modeling is less sensitive than NDVI to soil background effects. Furthermore, Drake (1991) and Adams et al. (1995) have shown that is possible to map the proportions of both green and nonphotosynthetic vegetation (NPV) using mixture modeling. This raises the possibility of estimating the different types of cover needed for the different applications outlined above. The green vegetation mixture map could provide information useful for input into models of evapotranspiration and for farm management purposes. Total vegetation cover [which can be obtained by adding the green, and NPV maps together (Drake, 1991)] provides information on land degradation and inputs into models of overland flow and erosion (Drake et al., 1995). To determine the utility of spectral matching and mixture modeling for rangeland vegetation cover estimation, we evaluated their precision over different rock and soil backgrounds and compared the results to that of two field techniques.

Rocks and Soils

Remote mineralogical identification and mapping has been an important goal of geological remote sensing for many years. Spectral matching and linear mixture modeling of imaging spectroscopy data have been shown to be effective methods of mapping the mineralogy of sparsely vegetated terrains (Clark et al., 1990; Kruse et al., 1993a; Ben-Dor and Kruse, 1995). Our study site provides a test of the utility of these methods in a semiarid region that contains a diverse geology including a sediment hosted gold deposit, and numerous areas of hydrothermally altered rocks that are partially covered in vegetation. However, the site is not as ideal for investigating the utility of these techniques for soil mapping because only one soil type is developed. We evaluated the effectiveness of these methods for mapping rocks and soil by determining the mineralogy of field samples and comparing them to image estimates of abundance and distribution.

Advantages and Limitations of Mixture Modeling of SWIR Data

Arguably the most important problem with linear mixture modeling is nonlinear mixing (Roberts et al., 1993). Linear mixing assumes that each photon has only interacted with one material in the image. This occurs when the materials are distributed as discrete units smaller than the resolution of the sensor that are physically or optically thick so that they transmit no light. Significant amounts of transmission leads to multiple scattering and nonlinear mixing.

Nonlinear mixing can be expected in vegetation canopies because for green vegetation transmission is high at certain wavelengths (Fig. 1a). By employing wavelengths where transmission is low, the assumption of linear mixing, though a simplistic one for vegetation canopies, is at its most valid. For SWIR wavelengths transmission of light by green leaves is variable but generally low because of absorption of light by water (Fig. 1a). After the visible it provides the wavelength range most appropriate for linear mixture modeling of green vegetation.

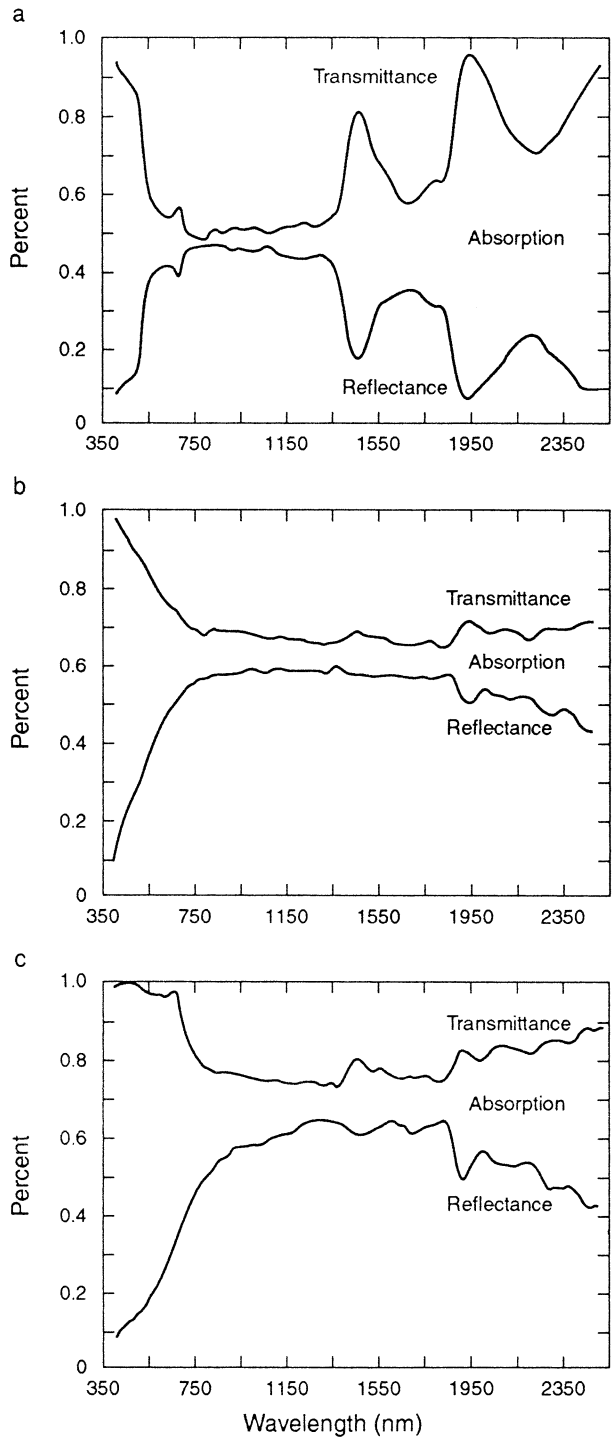

Figure 1. Reflection, absorption and transmission of light for a green and senesced soy bean leaf (after Jacquemoud, 1989): A) green leaf, B) yellow senescent leaf, and C) brown senescent leaf.

Transmission through woody material is unlikely due to its opaque nature, however, the transmission properties of leaves seem to vary at different stages of senescence. Transmission by yellow senescent leaves is about 30% throughout the SWIR (Fig. 1b) and thus may pose a problem, but is only about 15% for brown leaves (Fig. 1c). Thus on the whole SWIR wavelengths seem promising for mixture modeling of vegetation canopies.

When finding endmembers by matching image to library spectra in order to apply a mixture model, the model can be trained by using either library or image endmembers. Library endmembers have the advantage that they are known to be pure and thus proportions estimates are absolute whereas image endmembers may be impure and the proportions estimates relative. However, as image endmembers contain the noise of the imaging system, it may be possible to estimate the error associated with this noise from them (Settle and Drake, 1993). We assessed the utility of both approaches of training the model by determining the purity of identified endmembers. We calculated the errors and assessed their ability to provide a method for evaluating the utility of the mixture maps for the above mentioned applications. We also assess their use in guiding endmember selection.

AVIRIS STUDY SITE

Climate and Vegetation

The study site is located in central Nevada, USA. The topography of the region is typical of the great basin. The altitude varies between 1524 m in the valley floors, and 2794 m at the top of the Sanoma Range. The area is semiarid, receiving about 200 mm of precipitation per year. Some of this precipitation falls as snow during the winter months, particularly at higher altitudes where it may last much of the winter providing water in the summer for the ephemeral streams that drain these mountains.

The vegetation of the region is highly variable. The most extensive plant community is sagebrush semi-desert which is dominated by woody sagebrushes such as *Artemisia tridentata* but contains other shrubs in lesser amounts such as snakeweed (*Chrysothamnus viscidiflorus*). Associated plant species are grasses and subshrubs (West, 1981). The deciduous shrub community is restricted to the well-watered areas such as the headwaters of the major river valleys that drain the Sanoma Range. Unlike sagebrush semidesert, in summer months this community provides a dense canopy of green leaves. Finally, the graminaceous community is present in low amounts throughout the study area, and is dominant in seasonally well-watered areas where the other communities are absent because of human disturbance such as fires or clearance. During the summer months these grasses quickly die off and present a canopy of dense senescent leaves.

Economic Geology and Geomorphology

The study area exhibits a complex geology, and there is considerable debate as to whether the different rock formations of the region (Fig. 2) represent a continuous sequence of sedimentation, or are related to distinct oro-

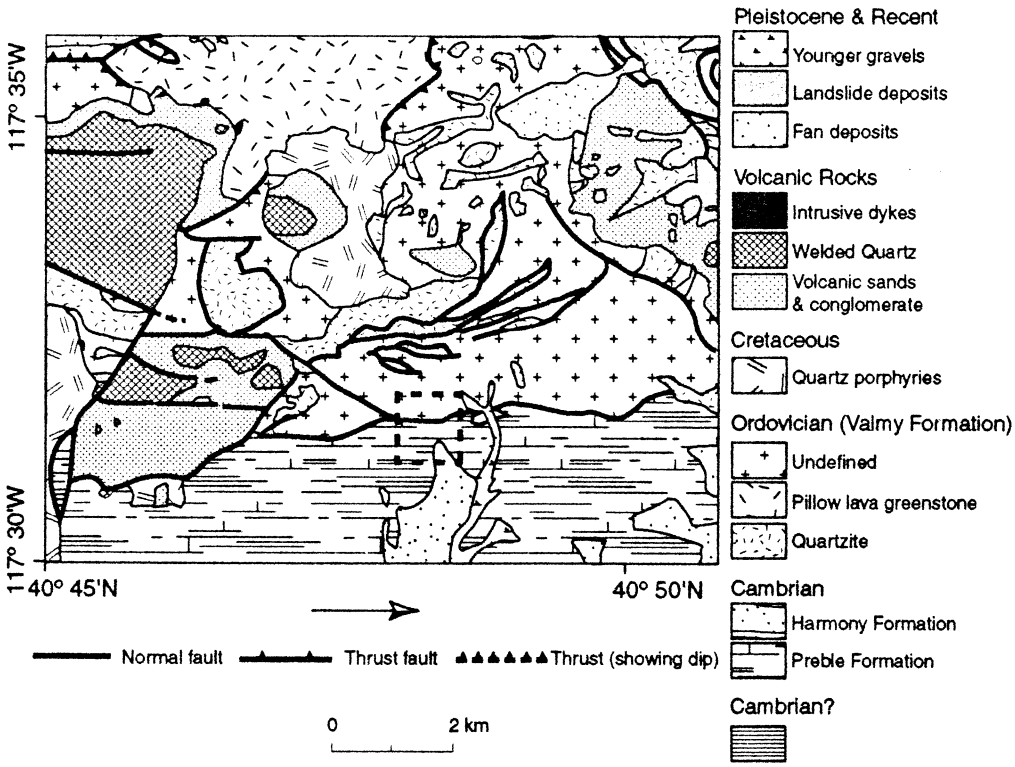

Figure 2. Geology of the study area. The region outlined by the dashed line defines the area shown in shown in Figure 4.

genic events (Madden-McGuire and Marsh, 1991). The geology has been studied in detail because of the numerous sediment-hosted disseminated gold deposits found along the Getchell trend. In the study area this trend expresses itself as a fault separating the Valmay and Preble Formations. The Preble Formation consists primarily of siltstone, micaceous phyllite, and quartsite with lesser chert, calcarious shale, sericite-ankerite schist, and limestone. The Valmay Formation consists primarily of chert, quartzite, and slate with localized areas of limestone which is sometimes silicified. A number of small intrusive bodies and quartz vein systems are associated with the Getchell Fault and some of its subsidiary splays, a few of which exhibit pyritic and argillic alteration. Gold mineralization is associated with this faulting and alteration, and one of these splays contains economic gold and silver mineralization that was being mined at the time of the AVIRIS over flight. Though the clay mineral illite is often directly associated with the gold in the sediment-hosted gold deposits of the region (Kruse and Hauff, 1991), most of the gold and silver in this mine is associated with the quartz vein systems; lower concentrations are found in quartz stockworks and the alteration zones that surround them (Dawson, 1988).

The outcrops of the above-mentioned rocks are mainly found on ridges, the valley sides and floor being covered by soil, colluvium, and alluvium. The soil is similar over all rock types, and is thought to originate from aeolian dust fallout derived from the surrounding playas (Chadwick and Davies, 1989).

EXPERIMENTAL IMAGERY

Two images were used in this study. The AVIRIS image was acquired in September 1990. Only the 35 AVIRIS SWIR bands from 2023.5 nm to 2374.1 nm were used in this analysis as the rest of the SWIR data contained too much noise. The synthetic image was created using spectra of 12 different materials(talc, epidote, pyrophyllite, alunite, muscovite, illite, calcite, kaolinite, gypsum, dolomite, montmorillonite, and NPV). Each material had a region of the image in which it was dominant but was linearly mixed with three other materials in up to four component mixtures. This was accomplished by dividing the image into 12 areas within which a single component was dominant. In each area the dominant component was assigned a value of 50% and up to four of the 12 materials were then randomly selected and assigned random proportions to make up the other 50% in each pixel. A small noise element due to nearest-integer-rounding errors is present in the data.

METHODS OF ANALYSIS

Data Preprocessing

The AVIRIS imagery presented many problems not expressed in the synthetic data set, the primary problem

being the many forms of random and systematic noise, which included horizontal striping effects, zero pixel values, and a generally low signal-to-noise ratio (20:1 for a 50% albedo target). In order to reduce this noise, a simple smoothing was performed using principal components analysis. This involved visually examining the principal component images, determining how many of them contain genuine information, and then inverting the transform using just those components. There is a somewhat subjective element in this as some principal components are dominated by noise but seem to contain a minor amount of spectral information. There were 35 bands in the original image, and the noise removal was based on the first eight of the principal components.

To calibrate the image, we processed it using the logarithmic residuals method (Green and Craig, 1985) to produce pseudoreflectance spectra that approximated true reflectance. The method provided a simple approach to obtain approximate reflectance curves, works well on scenes such as this where there is much spectral variation from pixel to pixel, but can produce unusual artefacts in the data. Another feature of logarithmic residuals is that it removes the brightness variations in the image caused by differences in grain size of rocks and soils, and factors such as shading due to surface roughness and the topography.

Linear Mixture Modeling

We use n to denote the numbers of spectral bands in the image, and c the number of cover types present. For any pixel, let x_i denote the observed signal in the ith multispectral channel, and let f_j denote the proportion of that pixel covered by the jth cover type. We write $x = \{x_1, x_2, \ldots, x_n\}^{\mathrm{T}}$ and $f = \{f_1, f_2, \ldots, f_c\}^{\mathrm{T}}$ (where the superscript T denotes "transpose"). The linear mixture model is defined by Eq. (1) (Horwitz et al., 1971):

$$x = Mf + e, \tag{1}$$

where M is an $(n \times c)$ matrix whose columns are endmember spectra. The quantity e is a noise term, which we take to have zero mean and variance–covariance matrix given by N, say. Assuming M and N are known, we can estimate f by a modified least squares approach, selecting that f that minimizes the quadratic function in Eq. (2):

$$(x - Mf)^T N^{-1} (x - Mf), \tag{2}$$

subject to the constraints

$$0 \leqslant f_i \leqslant 1, \qquad i = 1, \ldots, c \tag{3}$$

and

$$f_1 + f_2 \cdots f = 1. \tag{4}$$

Equation (3) states that the elements of f are nonzero and Eq. (4) that they add up to 1. If the errors are Gaussian, then this minimization gives the maximum likelihood estimate of f. The second constraint is straightforward to implement (e.g., Settle and Drake, 1993), but the first is more problematic. Shimabukuro and Smith (1991) present algorithms for the cases $c=3$ and 4, but these are not easily generalized, and, when more classes are present, we need to apply a quadratic programming approach (Settle and Drake, 1993) or adopt some suboptimal estimation method.

The prediction error on the estimated proportions vector is a random variable which has a mean of zero and a variance covariance matrix E (Settle and Drake, 1993). This is independent of f provided that e is itself independent of f. The square root of E_{ii}, the ith diagonal element of E, gives a measure of the prediction error on the ith component of f. As a simple illustrative example, consider the case of a two-component mixture, the endmembers of which are μ^1 and μ^2 , and for which random noise is uncorrelated and of equal variance in all channels (i.e., $N = \sigma^2 I$, where σ^2 is the variance and I is the $n \times n$ identity matrix). Then we find Eq. (5):

$$E_{11} = E_{22} = \sigma^2 / \|\mu^2 - \mu^1\|^2, \tag{5}$$

where $\|y\|$ denotes the length of an arbitrary vector y. Thus the prediction error in this two-component model is simply the noise level, divided by the spectral separation of the endmembers. The more general case is nothing so simple, but it remains true that the prediction error depends on the spectral separability of the endmembers, measured relative to the noise variance. Thus E provides a useful tool for assessing the likely effectiveness of any mixture analysis. For example, a value of E of 0.5 means that for 33% of the pixels the actual abundance will be $\geq \pm 50\%$ of the predicted pixel value; thus the pixel could have a value of 0% or 100% and in effect is undetectable by mixture modeling as it fills the entire range of percentages. Even an E of 0.25 will mean that the mixture map will be dominated by noise and will be of little practical value.

Though the E has been shown to be effective in evaluating errors using synthetic imagery (Settle and Drake, 1993), there have been few tests of the method on real data. Problems can be expected with the AVIRIS imagery as to calculate E there have to be enough endmember pixels to characterize the image noise, and pure pixels are rare in semiarid rangelands. Furthermore, the AVIRIS imagery contains both random and systematic noise and there is also likely to be some variation caused by minor changes in the spectral quality of endmembers from pixel to pixel. To derive absolute values of the prediction error, we need to know the image noise, and it has to be random. However, when this is not the case, as is likely with the AVIRIS imagery, we can assume a constant variance when calculating E and inspection of the matrix will still provide clues to the relative reliability of the proportions estimates, and also (via off-diagonal terms) to evidence of confusion between pairs of endmembers.

Spectral Matching

Spectral matching techniques are widely used in chemistry and other disciplines but have only recently been used as an analytical technique for imaging spectroscopy (Clark et al., 1990; Mackin et al., 1990). Each library spectrum is compared against the unknown image spectrum across the SWIR wavelength range after converting the library spectra to the same bandwidths as the image.

In order to match curve shape but not differences in reflectance, the library and the AVIRIS image spectra were normalized. Normalization helps compensate for topographic and grain size effects and the fact that many of the library spectra are hemispherical, whereas the image spectra are bidirectional. Our normalization converts reflectance spectra to variations about the mean of each spectrum, using Eq. (6):

$$D_i = \frac{x_i - \bar{x}}{\sum_{n=1}^{i} |x_i - \bar{x}|} \tag{6}$$

where D_i is the normalized value for band i, x_i the reflectance value for band i, $\bar{x}_i$ the mean value of the spectrum, and n the number of bands.

Image spectra were then matched to library spectra. There are a number of ways of doing this. We have used the following distance function [Eq. (7)]:

$$C_j = 1 - \sum_{i=1}^{n} |D_{ij} - D_i| \tag{7}$$

where D_{ij} is the normalized data value of band i for library spectrum j and D_i the normalized data value of band i for the unknown image spectrum. C_j varies between 1 and -1 for each of the j library spectra. Values of 1 represent a perfect fit, and values below zero are rejected as the fit is poor. The identity of the material with the highest C_j greater than zero is assigned to each image spectrum. The pixel that has the highest C_j will be the purest example of that material in the image. Thus as well as producing a classification map this method has potential for determining the number, identity, and location of the image endmembers.

If the spectra are normalized such that $\sum D_i^2 = 1$ and a euclidean distance used for comparison, the matching amounts to maximizing the standard cross-correlation of the normalized spectra, or equivalently to the so-called Spectral Angle Mapper (Kruse et al., 1993b). The D_i metric was preferred in this study because it is more robust.

Field Validation of AVIRIS Imagery

In order to check that the minerals identified in the imagery were actually present on the ground, 20 samples were collected, and their mineralogy determined by x-ray diffraction (XRD). Sample sites were selected with reference to geological maps and field work with the aim of sampling the mineralogical diversity of the region. In order to relate the XRD results to the results of the spectral matching and linear mixture, modeling sites with homogeneous geology or soil exposure and low or absent vegetation cover were selected.

Vegetation cover was measured using two methods and two observers in order to quantify the errors associated with these field estimates as well as those associated with the mixture modeling. The first approach used the line intercept method using three random 30 m transects taken from a stake. Only senescent and green vegetation proportions could be easily distinguished using this method as it proved hard to define the size of the smaller plant parts such as sagebrush flowers and grass stems.

In order to record the abundance of these smaller canopy components, a vertical photograph approach was adopted. This involved taking a vertical photograph every 5 m along each of the three transects. Slides were then projected onto a gridded screen that contained 100 cross points with the canopy component at each cross point noted and converted to a percentage. The components we considered were green leaves, grey bark, brown bark, flowers, senescent leaves, senescent grass, soil, and litter (grey wood, grey grass, cow dung). Samples of the different plant parts were collected and their spectra acquired using a Geophysical Environmental Research Corporation single field of view spectroradiometer (GER SIRIS) and a Beckman 5240 Spectroradiometer equipped with an integrating sphere.

RESULTS

Spectral Matching

Spectral Matching the Synthetic Image

Spectra from the Jet Propulsion Laboratory (JPL) and the International Geological Correlation Programme (IGCP) spectral libraries was used for analysis of the imagery. The synthetic image was matched to a sublibrary containing 20 materials, 12 of which existed in the image. The pixels with the highest match scores were the purest pixels of each of the 12 materials in this image. No other spectra in the library exceeded the match score threshold of zero. Misclassification was evident in the maps of the matched pixels whereby a few were assigned to materials that did not exhibit the highest proportion in that pixel. These errors occur when high contrast spectra are mixed with spectra of lower contrast. In this situation the high contrast spectrum dominates the mixed spectrum, and thus the matching assigns the pixel to the high contrast material.

Spectral Matching the AVIRIS Image

A sublibrary containing 23 minerals and two vegetation spectra was used to analyze the AVIRIS image (Table 1). Twelve minerals provided match scores below the threshold of zero, and were deemed to be absent; nine mate-

Table 1. Library Spectra Matched to the AVIRIS Imagery

Indentified as Contagious Units	*Identified as Scattered Pixel*	*Not Identified*
Muscovite	Jarosite	Magnesite
Illite	Epidote	Actinolite
Calcite	Clinozoisite	Tremolite
Dolomite	Hematite	Alunite
Kaolinite	Chlorite	Brucite
Gypsum	Goethite	Pyrophyllite
Montmorillonite		Talc
Green vegetation		Dickite
NPV		Saponite

rials provided high match scores that formed spatially contiguous units, and are likely to be present; and six minerals provided match scores that exceeded the threshold but were rare and exhibited no spatial pattern. Investigation of the image spectra for the latter pixels showed that the match score exceeded the threshold because noise in the image spectra can sometimes cause sudden peaks or dips in reflectance that mimic reflectance peaks and absorption features in the library spectra. Materials that showed this random spatial pattern were therefore ignored.

Vegetation: The map of pixels that exceed the match score threshold for green vegetation predominantly outlined dense stands (90–100% cover) of the annual shrub community while those of NPV predominantly mapped areas of dense senescent grass cover (90–100%). These maps of vegetation provide little information on the sagebrush shrub community as the vast majority of pixels are mixed. This mixing occurs at two scales. First, the patchy distribution of shrubs provides areas of exposed ground between individual plants. Second, the shrub canopies themselves are sparse and heterogeneous, containing numerous different plant parts in different proportions (Table 2).

We investigated the spectral variation of these different plant parts in the canopy for sagebrush and snakeweed (Fig. 3). Though the spectra of snakeweed green leaves and live flowers differ markedly in reflectance in the visible, they are remarkably similar in terms of both reflectance and curve shape in the SWIR (Fig. 3a). Sagebrush flowers and leaves also exhibit differences in reflectance in the visible; however, the flowers have a much lower reflectance in the near-infrared but are similar in the SWIR. Thus in the SWIR the flowers and leaves exhibit a similar spectral curve shape for both species. The logarithmic residual transformation of the AVIRIS data, and the normalization associated with the matching procedure mean that we are only using curve shape in our analysis, and thus flowers can be expected to be confused with green leaves. However, as snakeweed is uncommon and the cover of flowers in dense sagebrush canopies is only 0.03%, the problem is minimal at this time of year.

Dry grass, grey wood, and brown wood exhibit a markedly different spectral response in the visible, and NIR because of lignin weathering (Fig. 3b) (Elvidge, 1990). However, the spectral curve shape of dry grass and these nonphotosynthetic plant materials is similar in the 2000–2400 nm region, where they all show absorption features due to lignin and cellulose (Elvidge, 1990). It appears that a number of different endmember spectra are needed to explain the spectral variation of NPV in the visible and NIR; however, most of these materials do not exhibit high proportions (Table 2) and thus may not form image endmembers. In the SWIR all these nonphotosynthetic plant materials exhibit similar spectral features, and, as a first-order approximation, they can be explained by a single endmember. In this image this endmember is dry grass because it is the only nonphotosynthetic plant material that exhibits 100% cover.

Rocks: Spectral matching suggests that muscovite, kaolinite, illite, and gypsum are primarily found in a small area of the Preble formation in the vicinity of the

Table 2. Variability the Proportions (%) of the Materials Visible within 1 m^2 Meter Areas of Sagebrush in Different Stages of Development

	Dense Canopy	*Sparse Canopy*	*Dead Canopy*	*Average of Region*
Canopy				
Green leaves	34	18.6	0.5	10.6
Senescent leaves	11.5	6.3	0	2.2
Brown bark	3.5	3.6	0	1.4
Grey bark	32	44	62.5	23.1
Live flowers	1.5	1.3	0	0.03
Under canopy				
Senescent grass	10.5	20.6	25.5	26.2
Soil	4.5	3.6	9	19.69
Litter				
Grey wood	0	1	0	5.3
Grey grass	0	1.6	0	10.1
Cow dung	0	0	0	1.1

gold mine. This area was intensively sampled in the field and XRD analysis confirmed the presence of extensive muscovite, and minor amounts of kaolinite (Table 3). We could not distinguish illite from muscovite in these samples using XRD because of the presence of numerous other minerals. In addition, our sampling provided no specimens that contained montmorillonite. However, there is independent evidence for the presence of illite, and montmorillonite in the vicinity of the mine (Dawson, 1988).

The geology of the region (Madden-McGuire and Marsh, 1991; Dawson, 1988), fieldwork, and XRD results do not support the presence of gypsum. This misclassification can be attributed to the fact in the SWIR the spectrum of gypsum is similar to a mixture spectrum of kaolinite and muscovite.

Muscovite/illite and kaolinite exhibit a considerable variation in the proportions for different samples collected within a single pixel (Table 3, D16a,b,c); thus it is hard to quantitatively relate the XRD results to the match scores. However, those regions that have high match scores for a mineral do seem to exhibit high proportions, but the samples are far from pure (Table 3). Quartz is the predominant mineral (usually >50%) with subordinate amounts of muscovite/illite and kaolinite. These quartz rich specimens still retain the spectral features of the less common clays because quartz is transparent, and spectrally featureless in the SWIR. In consequence, the clay endmembers defined by spectral matching cannot be considered "pure," even though they match well to pure laboratory spectra. Thus there is no advantage in using library spectra as endmembers as the proportions estimates derived from the mixture modeling using these endmembers will still be relative not absolute and *E* cannot be calculated. The only way to determine the actual mineral concentrations in these endmember pixels is to conduct intensive sampling and mineralogical analysis; however, for mineral exploration purposes, ac-

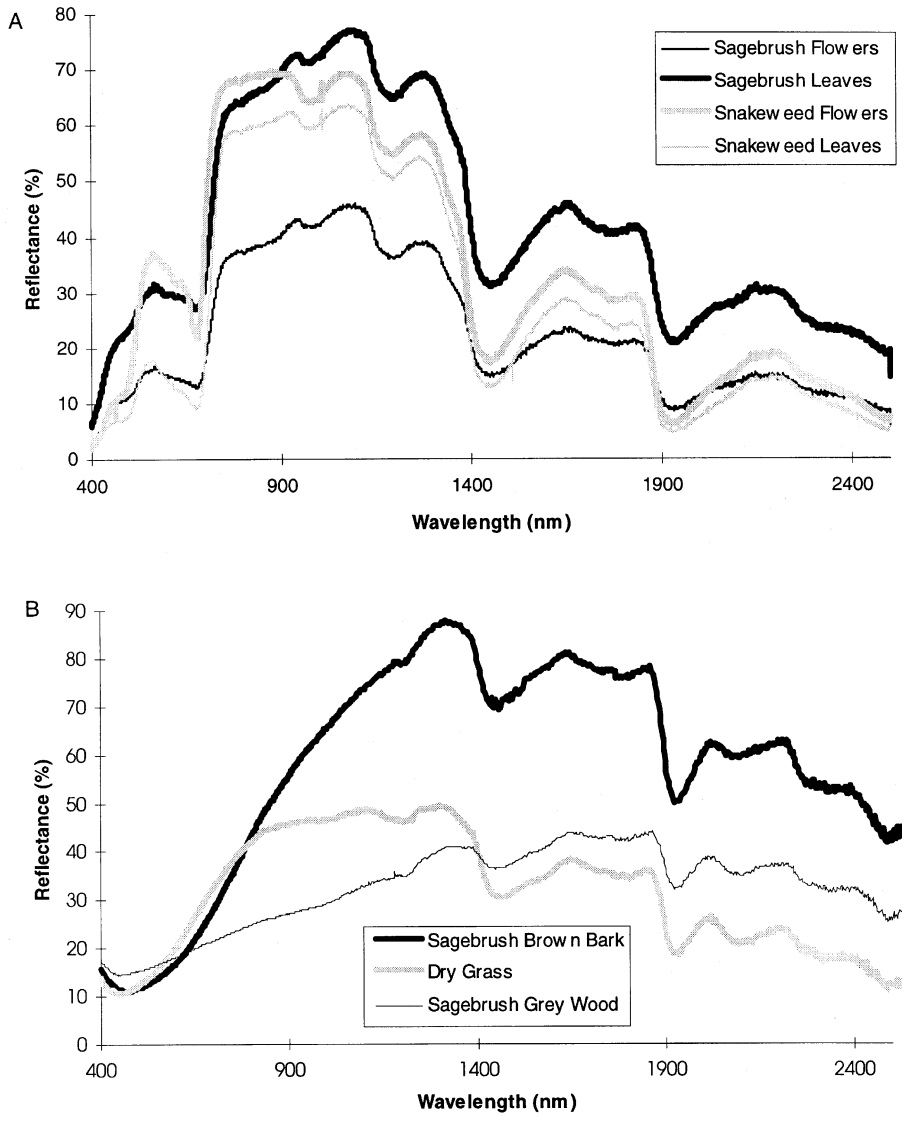

Figure 3. Spectra of the different plant parts found in the sagebrush and snakeweed canopy: a) live plant parts; b) woody plant parts.

Table 3. XRD Analysis of Selected Rock and Soil Samples[a]

Sample Site and Type	*Muscovite and/or Illite (%)*	*Kaolinite (%)*	*Quartz (%)*	*Orthoclase and Plagioclase Feldspars (%)*	*Amphibole (%)*	*Other (%)*
Soils						
D1	14.4	2.5	47.7	19.7	2.2	Zeolite 14.1
D8	17.9	5	45.1	23.4	0.4	Zeolite 8.2
D11	19.9	16.5	33.8	28.3	1.4	
D12	16	5.3	52.1	25.2	1.4	
D13	18	3.6	59.7	11.5	0.4	
D14	17.9	7.6	57.2	13.5	0.4	Zeolite 3.4
AM2	6.2		39.8	9.5		Calcite 41.2
Rocks						
D1	42		51.2	1		Haematite and/or Goethite 3.4 Lepidocrocite 1.4
D8	6.3	16.3	76.5			Lepidocrocite 0.9
D11	6.8	15.5	74.2		0.8	
D12			16.8			Ankerite 83.2
D13	31.5		68.5			
D14	47.3	24.9	27.8			
D16a	32.1		67.9			
D16b			100			
D16c	26.6	5.2	68.2			
D18			12.4			Calcite 87.6
J1			7.8			Calcite 92.2

[a]We could not distinguish illite from muscovite in these samples using XRD because of the presence of numerous other minerals.

curate estimates of proportions are not necessary as it is the spatial association of minerals that provides the best indicator of potential gold mineralization.

The distribution of calcite and dolomite was confined to extensive areas in the west that contain limestone outcrops but could not be verified due to access restrictions and to a series of carbonate hills in the northeast part of the image. These carbonate hills were closely studied on the ground, and XRD showed the limestone to be predominantly calcite as suggested by spectral matching (Table 3). For calcite the highest match scores corresponded to rock outcrops that contained about 90% calcite and 10% quartz (Table 3, samples D18 and J1); thus, in the case of calcite, almost pure pixels are being identified as such by the matching procedure.

Despite the identification error of gypsum and the fact that high match scores do not correspond to pure deposits for some minerals, the map of mineral zonation provided by the spectral matching is extremely useful for targeting new areas of alteration associated with quartz veins that may contain mineralization (Fig. 4). The ability of the methodology to map the different minerals produced by hydrothermal alteration provides a very useful mineral exploration tool, though subsequent exploration drilling in this region did not ultimately reveal further economic gold mineralization. Furthermore, the ability to distinguish illite from muscovite provides a powerful tool for locating other sediment hosted gold deposits because of the common association of gold with illite.

Soils: Few areas of soil were mapped by spectral matching primarily because they are only well developed on the valley bottoms, and in these regions they are covered in vegetation. Many of the minerals found in the soils are the same as those found in the surrounding rocks, and thus appear to be largely locally derived (Table 3). The exceptions are the feldspars, amphiboles, and zeolites, which are found only in the soils. The former two minerals probably represent transported material, and the latter a weathering product. The commonest of these components is the feldspars. Like quartz, feldspar minerals have no diagnostic spectral features in the SWIR (Grove et al., 1992). The soil spectra appear to show variations in the size, and shape of the absorption feature at 2.2 μm due to variations in the amount of illite, muscovite, and kaolinite (Fig. 5), while the other mineralogical variations are not evident in the spectra. Thus areas of high soil exposure are mapped by the spectral matching according to their clay content.

Mixture Modeling

The image endmembers defined by the matching procedure were used in preference to library endmembers to mixture model both the synthetic and AVIRIS images for three reasons. First, we have shown that clay endmembers are not pure, even though they match well to pure library spectra. Second, image endmembers contain noise, and thus allow calculation of the errors associated with the proportions estimates (E), as long as there are

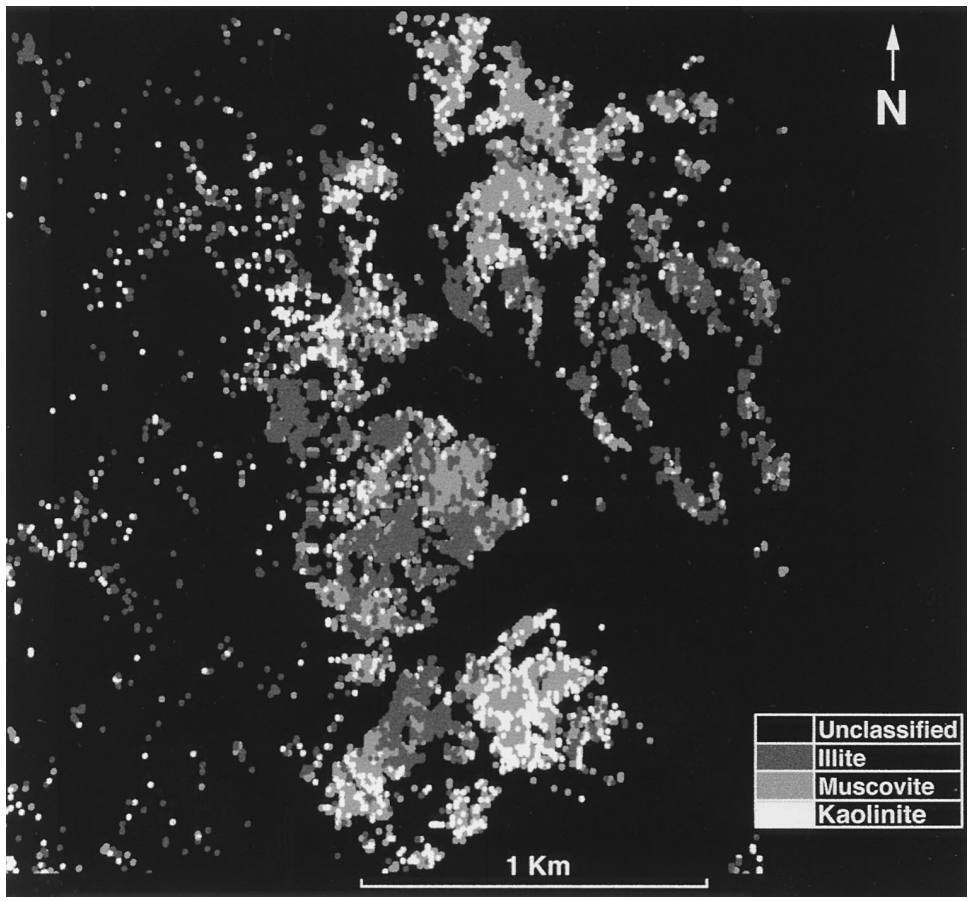

Figure 4. The results of spectral matching for a region of hydrothermal alteration in the vicinity of the Getchell fault. The location of this image is outlined in Figure 2. Black areas represent mixed pixels that are unclassified as they fall below the threshold. Areas of illite/muscovite zoning offer the highest potential for the presence gold mineralization.

enough pixels to characterize this noise. Third, because of the sensitivity of mixture modeling to noise, high noise levels affects the ability of mixture modeling to utilize low contrast endmembers because they are swamped by it (Sabol et al., 1992). *E* can be used to quantify this detectability as it quantifies the effects of noise outlined by Sabol et al. (1992). Recall that a value of *E* of 0.50 translates to a fractional error $\geq \pm 50\%$ for 33% of the image pixels and thus a pixel could actually have a value of 0% or 100% and in effect is undetectable.

Mixture Modeling the Synthetic Image

The synthetic image provides a baseline because all endmembers are represented by numerous pure pixels and the only noise present is due to rounding from real to byte. The errors are therefore due to quantization and differences in contrast, and show what can be achieved in the absence of system noise. *E* is small in general; however, there are notable errors on the proportions estimates for some materials (Table 4). The largest *E* is that of NPV where we can expect 33% of the proportions estimates to be $\geq \pm 5.4\%$ of the predicted pixel value even in this favorable situation.

Mixture Modeling the AVIRIS Image

Much higher errors were found using AVIRIS imagery, which has a much higher signal-to-noise ratio. When the nine endmembers defined by the spectral matching were applied to the image, all the mixture maps were heavily influenced by noise, and some endmembers had to be discarded by dropping those with the highest *E* (Table 4). Unfortunately, due to the lack of pure pixels identified by the matching procedure, it was not possible to characterize the image noise, and produce precise values for *E*. To alleviate this problem, a constant value (1DN) was assumed for the noise; thus *E* only provided a measure of the contrast between the endmember spectra.

By successively dropping the endmember with the highest *E*, recomputing *E*, and inspecting the mixture maps for the influence of noise, it proved possible to ensure that the lowest contrast endmembers were discarded. However, by ignoring materials that are known to exist, confusion is inevitable. By coupling this procedure with the maps of the distribution of materials provided by the spectral matching, this confusion can be monitored and is outlined in Table 4. Generally, if two minerals had similar absorption features, then both exhibited a high *E*, the one with the highest was dropped, and confusion occurred between them. The exception is kaolinite, which has a spectrum that differs markedly from the other clay minerals found in the region while illite and muscovite exhibit similar spectral features. However, kaolinite has a higher *E* than illite in the six end-

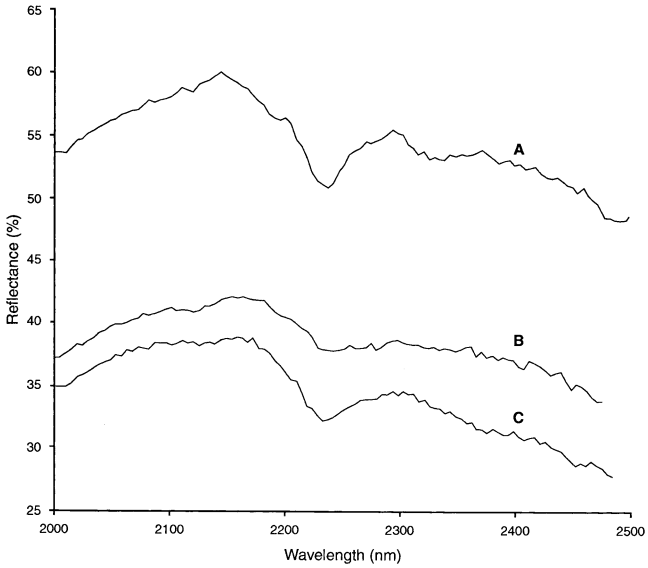

Figure 5. SWIR spectra of the soils with various amounts of illite/muscovite and kaolinite. Spectrum A contains 36.5% clay (19.9% muscovite/illite and 16.5% kaolinite), spectrum B contains 10.5% clay (7.3% muscovite/illite and 3.2% kaolinite), and spectrum C contains 21.3% clay (16% muscovite/illite and 5.3% kaolinite).

member solution and was dropped. This occurs because the kaolinite endmember is far from pure; no samples we collected contained more than 24.9% whereas the other clays are found in higher amounts.

For NPV and green vegetation, changes in both the influence of noise on the mixture maps and the magnitude of the proportions estimates occurred as the number of endmembers was reduced, even though they always provided a lower *E* than discarded endmembers. For the green vegetation with five endmembers the proportions estimates were largely free from noise, and appeared to be realistic as high proportions were restricted to the river valleys where the annual shrub community is found. However, for NPV much noise was still evident though areas of high an low cover could be discerned.

In general, the magnitude of *E* reflected either the amount of noise evident in the mixture maps, or the cases when the materials were grossly under- or overestimated. These results suggest that mixture modeling is much more susceptible to noise than spectral matching. Confusion between spectrally similar endmembers is an inevitable consequence of noisy data, and, even with a small number of endmembers, noise exerts a significant influence on the proportions estimates of the lowest contrast materials.

As with the rocks, problems were found when trying to quantitatively validate the mixture modeling vegetation cover estimates. To determine the advantages and limitations of remote sensing approaches to measuring vegetation cover, we need to compare them to the pros and cons of the ground measurements themselves. Holm et al. (1984) found large differences between different methods of measuring vegetation cover on the ground and between different observers using the same techniques. Any field survey that covers the same number of sites as the AVIRIS imagery (313,344 pixels) would need to use more than one observer. By employing two methods of estimating vegetation cover in the field, and in one case two observers, it was possible to gain a limited insight into the errors associated with the field measurements. We found an 8% difference in total cover estimates between observers interpreting the same photographs, but a 40% or more difference between the two methods of vegetation cover estimation implemented by the same observer. Table 5 shows the comparison of all sites and all methods. The photographic line intercept provides consistently higher cover than the line intercept

Table 4. Error on the Proportions Estimates (*E*) for A) the Synthetic Image, B) the Nine Endmember Mixture Analysis of AVIRIS Data, C) the Seven Endmember Mixture Analysis of AVIRIS Data, D) the Six Endmember Mixture Analysis of AVIRIS Data, E) the Five Endmember Mixture Analysis of AVIRIS Data[a]

Material	*A*	*B*	*C*	*D*	*E*	*Confusion*
Talc	0.009					
Epidote	0.014					
Pyrophyllite	0.008					
Alunite	0.013					
Muscovite	0.018	0.106	0.078	0.056	0.029	
Illite	0.037	0.153	0.087	0.036	0.036	
Calcite	0.015	0.257	0.019	0.013	0.009	
Kaolinite	0.015	0.242	0.109	0.067	Drop	Muscovite
Gypsum	0.024	0.246	0.099	Drop	—	Muscovite
Dolomite	0.017	0.267	Drop	—	—	Calcite
Montmorillonite	0.012	0.297	Drop	—	—	Muscovite
NPV	0.054	0.192	0.016	0.016	0.015	
Green vegetation	—	0.128	0.028	0.027	0.009	

[a] The confusion column shows which material the discarded endmember was confused with.

Table 5. Accuracy Assessment for Mixture Modeling Estimates of Vegetation Cover

Background	*Site 1 Soil and Litter*	*Site 2 Calcite*	*Site 3 Muscovite*	*Site 4 Kaolinite*	*Average Absolute Difference*
Total vegetation cover					
Photographic line intercept as ground truth	87	10.5	21	15.5	
Line intercept	40.3	8.6	13.9	9.3	14.0
Mixing	66.1	39.4	6.4	5.4	18.9
Line intercept as ground truth	40.3	8.6	13.9	9.3	
Photographic line intercept	87	10.5	21	15.5	14
Mixing	66.1	39.5	6.4	5.4	17.3
Green vegetation cover					
Photographic line intercept as ground truth	13	2.5	7	4.0	
Mixing	3.6	2.1	6.4	4.2	2.7
NPV cover					
Photographic line intercept as ground truth	74	8	14	11.5	
Mixing	62.5	37.4	0	1.2	16.2

due to the fact that the former technique is better at including small plant parts in the cover estimates; however, the results of the mixture modeling shows no consistent pattern.

The average absolute difference between the "ground truth" and the mixture model results has been calculated to provide a single figure estimate of precision. As there are clearly problems in deciding what is the truth on the ground, these figures have been calculated using each ground-based method as the truth. It is clear that the differences in total cover estimates between all three techniques is high. It is marginally lower between the two field estimates (±14%) than between either of the field estimates, and the mixture model estimates (±17.3 and ±18.9). However, because the ground estimates used in this calculation were acquired by one observer, the loss of precision due to different observers is not considered in these figures so that the errors for the field measurements are underestimates.

Table 5 also shows the precision of the green and NPV cover estimates individually. Though the number of validation sites is too small to draw firm conclusions, green vegetation cover estimates seem to be remarkably precise considering that proportions are low and each site exhibits a different background. NPV cover estimates are poor, however, and this can be largely explained by the noise evident in the NPV mixture map. The difference in precision of the green and NPV cover estimates is anticipated by *E* underlining its utility as an indication of mixture model performance even when there are too few pixels to characterize the noise.

The high errors associated with NPV limit the usefulness of mixture modeling for the applications that need total vegetation cover outlined in the second section. This raises the question, "is it possible to accurately estimate NPV cover using mixture modeling of SWIR imaging spectroscopy data?". Table 6 summarizes the limited literature on the errors associated with green and NPV proportion estimation using SWIR wavelengths. The results show that these estimates are highly sensitive to quantization, and other noise effects and that NPV is extremely hard to estimate accurately. The synthetic im-

Table 6. Summary of the Literature on Estimates of the Errors Associated with Green and NPV Proportion Estimation[a]

E *for Green Vegetation*	E *for NPV*	*Number of Materials in Image*	*Noise and Quantization*	*Image Type*	*Source*
0.084	0.181	5	SNR 50:1 for 50% albedo	GER	Mackin et al. (1990)
0.119	0.260	7	SNR 50:1 for 50% albedo	GER	Mackin et al. (1990)
0.256	0.389	6	Rounding from real to byte	Synthetic	Drake (1992)
0.266	0.404	6	Rounding from real to byte + 1 DN noise	Synthetic	Drake (1992)

[a]The GER image was acquired by the GER imaging spectrometer.

age used in this study produced a low *E* for NPV when compared to those in Table 6. Much higher errors were found by Settle and Drake (1993) in a similar situation where quantization was the only form of noise. The large difference in the *E* for NPV between the two images must be due to a difference in the contrast, showing that the precision of NPV proportion estimation is highly scene-dependent.

Though these results suggest that the precision of NPV cover estimates, and thus total vegetation cover, is poor, so are field estimates. Though it is hard to improve on field estimates (Holm et al., 1984), it is easy to suggest ways of improving remote sensing estimates. The factors that can be manipulated to improve the precision of mixture modeling NPV cover estimates are noise, quantization, spectral range, and spectral resolution. As the signal-to-noise ratio of AVIRIS has consistently improved since our data were acquired, better cover estimates should now be obtainable; however, a scanner with a very high signal-to-noise ratio collecting real data is probably needed to consistently acquire precise NPV cover estimates.

CONCLUSIONS

SWIR wavelengths have been shown to be useful for mapping both surface mineralogy and vegetation in semiarid shrublands, although the low signal-to-noise ratio of AVIRIS SWIR data introduced problems. Spectral matching and linear mixture modeling provided complementary mapping tools as spectral matching was a useful method for locating and identifying endmembers as well as being a useful mapping tool in its own right. However, both methods encountered problems.

Spectral matching identified gypsum when it was not actually present. Furthermore, though the vegetation endmembers defined by spectral matching were located in regions of 100% cover, the clay endmembers, though matching well with pure library spectra, did not correspond to pure outcrops when investigated on the ground. Quartz was the predominant mineral while the identified clay minerals never exceeded 50%. With impure endmembers the mixture modeling proportions estimates were thus relative, not absolute.

Notwithstanding this limitation, spectral matching provided maps that were extremely useful for geological mapping and mineral exploration. It was more effective than mixture modeling at mapping relatively pure outcrops of the numerous minerals present in the area because it was more robust in the presence of noise. This noise necessitated discarding endmembers during mixture modeling thus causing confusion. The error measure (*E*) provided a useful statistic for deciding which endmembers to discard in order to reduce the effect of noise on the mixture maps. However, the lack of pure pixels meant that it could not be used to provide a quantitative measure of the precision of the mixture model.

For vegetation, mixture modeling supplied more useful information than spectral matching did as the applications outlined in the second section require abundance estimates of vegetation for all image pixels, but spectral matching only outlined a few areas of high NPV and green vegetation cover. The spectra of the different plant parts showed that, though they exhibit large differences in reflectance in the visible and near-infrared, in the SWIR the canopies can be approximated adequately as a mixture of an NPV component and a green vegetation component. Though mixture modeling estimates of green vegetation cover were precise, NPV cover estimates, and thus total vegetation cover, showed poor precision as they were heavily influenced by noise.

Steve Briggs, the British National Space Centre (BNSC), and Reading University are thanked for funding the field work and image acquisition. Thanks also to Steve Plummer for help in the field and calculation of some of the vegetation cover estimates, and to Chris Elvidge for helpful discussions on the vegetation of Nevada and for providing access to a spectroradiometer.

REFERENCES

Adams, J. B., Sabol, D. E., Kapos, V., et al. (1995), Classification of multispectral images based on fractions of endmembers: application to land-cover change in the Brazilian Amazon. *Remote Sens. Environ.* 52:137–154.

Ben-Dor, E., and Kruse, F. A. (1995), Surface mineral mapping of Makhtesh Ramon Negev, Israel using GER 63 channel scanner data. *Int. J. Remote Sens.* 16:3529–3553.

Chadwick, O. A., and Davies, J. O. (1989), Soil-forming intervals caused by eolian sediment pulses in Lahotan basin, northwestern Nevada. *Geology* 18:243–246.

Clark, R. N., Gallagher, A. J., and Swayze, G. A. (1990), Material absorption band depth mapping of imaging spectrometer data using a complete band shape least-squares fit with library reference spectra. In *Proceedings 2nd Airborne Visible/Infrared Imaging Spectrometer (AVIRIS) Workshop*, JPL Publication 90-54, Jet Propulsion Laboratory, Pasadena, CA, pp. 176–186.

Dawson, J. M. (1988), The Adelaide Crown property Humbolt County, Nevada, Report, Getchell Resources Inc., Kamloops, British Colombia, Canada.

Drake, N. A. (1991), Mapping, rocks, soils, vegetation communities and vegetation density with the GERIS using linear mixture modeling and post-processing techniques. *ERSeL Adv. Remote Sens.* 1:42–56.

Drake, N. A. (1992), Mapping and monitoring surficial materials, processes and landforms in southern Tunisia using remote sensing, Ph.D. thesis, University of Reading, United Kingdom.

Drake, N. A. Vafeidis, A. Wainwright, J., and Zhang, X. (1995), Modelling soil erosion using remote sensing and GIS techniques. In *Proceedings of RSS 95 Remote Sensing in Action*, 11–14 September, Southampton, pp. 217–224.

Elvidge, C. D. (1990), Visible and infrared reflectance characteristics of dry plant materials. *Int. J. Remote Sens.* 12:1775–1795.

Elvidge, C. D., and Chen, Z. (1995), Comparison of broad-band and narrow band read and near-infrared vegetation indices. *Remote Sens. Environ.* 54:38–48.

Elvidge, C. D., and Lyon, J. R. P. (1985), Influence of rock-soil spectral variation on the assessment of green biomass. *Remote Sens. Environ.* 17:265–279.

Frank, A. B., and Aase, J. K. (1994), Residue effects on radiometric reflectance measurements of northern Great Planes rangelands. *Remote Sens. Environ.* 49:195–199.

Garcia-Haro, F. J., Gilabert, M. A., and Melia, J. (1996), Linear spectral mixture modeling to estimate vegetation amount from optical spectral data. *Int. J. Remote Sens.* 17:3373–3400.

Graetz, R. D., Pech, R. P., Gentle, M. R., and O'Callaghan, J. F. (1986), The application of Landsat image data to rangeland assessment and monitoring: the development and demonstration of a land image-based resource information system (LIBRIS). *J. Arid Environ.* 10:53–80.

Green, A. A., and Craig, M. D. (1985), Analysis of aircraft spectrometer data with logarithmic residuals. In *Proceedings of the Airborne Imaging Spectrometer Workshop*, JPL Publication 85-41, Jet Propulsion Laboratory, Pasadena, CA, pp. 111–119.

Grove, C. I., Hook, S. J., and Paylor, E. D., II (1992), Laboratory reflectance spectra of 160 minerals, 0.4 to 2.5 micrometers, JPL Publication 92-2, Jet Propulsion Laborartory, Pasadena, CA.

Holm, A. R., Curry, P. J., and Wallace, J. F. (1984), Observer differences in transect counts, cover estimates and plant size measurements on range monitoring sites in an arid shrubland. *Austr. Rangeland J.* 6:98–102.

Hook, S. J., Elvidge, C. D., Rast, M., and Watanabe, H. (1991), Evaluation of short-wave-infrared (SWIR) data from the AVIRIS and Geoscan instruments for mineralogical mapping at Cuprite, Nevada. *Geophysics* 56:1432–1440.

Horwitz, H. M., Nalepka, R. F., Hyde, P. D., and Morganstern, J. P. (1971), Estimating the proportion of objects within a single resolution element of a Multispectral Scanner. University of Michigan, Ann Arbor, Michigan, NASA Contract NAS-9-9784.

Huete, A. R., Jackson, R. D., and Post, D. F. (1985), Spectral response of a plant canopy with different soil backgrounds. *Remote Sens. Environ.* 17:37–55.

Jacquemoud, S. (1989), Modelisation des proprietes optiques des feuilles, Diploma Thesis, Institut National de la Recherche Agronomique, Montfavet, France.

Kennedy, P. J. (1989), Monitoring the phenology of Tunisian grazing lands. *Int. J. Remote Sens.* 10:835–845.

Kruse, F. A., and Hauff, P. L. (1991), Identification of illite polytype zoning in disseminated gold deposits using reflectance spectroscopy and x-ray diffraction-potential for mapping with imaging spectrometers. *IEEE Trans. Geosci. Remote Sens.* 29:101–104.

Kruse, F. A., Lefkoff, A. B., and Dietz, J. B. (1993a), Expert system-based mineral mapping in northern Death Valley, California/Nevada, using the airborne visible/infrared imaging spectrometer (AVIRIS). *Remote Sens. Environ.* 44:309–336.

Kruse, F. A., Lefkoff, A. B., Boardman, J. B., et al. (1993b), The spectral image processing system (SIPS)—interactive visualization and analysis of imaging spectrometer data, *Remote Sens. Environ.* 44:145–163.

Mackin, S., Drake, N. A., Settle, J. J., and Rotfuss, H. (1990), Towards automatic mapping of imaging spectrometry data using an expert system and linear mixture model. In *Proceedings 5th Australasian Remote Sensing Conference*, 8–12 October, Perth, Western Australia.

Madden-McGuire, D. J., and Marsh, S. P. (1991), Lower Paleozoic host rocks in the Getchell gold belt: several distinct allochthons or a sequence of continuous sedimentation? *Geology* 19:489–492.

Pickup, G., Bastin, G. N., and Chewings, V. H. (1994), Remote sensing based condition assessment for nonequilibrium rangelands under large-scale grazing. *Ecol. Appl.* 4:494–517.

Ringrose, S., Matheson, W., Matlala, C. J. S. S., and O'Neill, T. (1994), Vegetation spectral reflectance along a north–south vegetation gradient in northern Australia. *J. Biogeogr.* 21:33–47.

Roberts, D. A., Smith, M. O., and Adams, J. B. (1993), Green vegetation, nonphotosynthetic vegetation, and soils in AVIRIS data. *Remote Sens. Environ.* 44:255–269.

Settle, J. J., and Drake, N. A. (1993), Linear mixing and the estimation of ground cover proportions. *Int. J. Remote Sens.* 14, 1159–1177.

Sabol, D. E., Adams, J. B., and Smith, M. O. (1992), Quantitative subpixel spectral detection of targets in multispectral images. *J. Geophys. Res.* 97:2659–2672.

Smith, M. O., Ustin, S. L., Adams, J. B., and Gillespie, A. R. (1990), Vegetation in deserts I: a regional measure of abundance from multispectral images. *Remote Sens. Environ.* 31:1–26.

Shimabukuro, Y. E., and Smith, J. A. (1991), The least-squares mixing models to generate fraction images derived from remote-sensing multispectral data. *IEEE Trans. Geosci. Remote Sens.* 29:16–20

West, N. E. (1981), Great Basin-Colorado Plateau sagebrush semi-desert. In *Arid Land Ecosystems: Functioning and Management* (D. W. Goodall and R. A. Perry, Ed.), Cambridge University Press, Cambridge, Vol. 2, pp. 331–349.